Seventh National Conference on Computational mechanics, Trondheim, 13-14 May, 2013
In: Skallerud B., Andersson H.I., editors. Computational mechanics, Trondheim, p. 159-178 (2013)

Numerical simulation of turbulent flames using the Eddy Dissipation Concept with detailed chemistry

Dmitry Lysenko, Ivar S. Ertesvåg
e–mail: dmitry.lysenko@ntnu.no
Department of Energy and Process Engineering
The Norwegian University of Science and Technology, Trondheim, Norway

Kjell Erik Rian
Computational Industry Technologies AS, N-7462 Trondheim, Norway

Bjørn Lilleberg
GexCon AS, NO-5892, Bergen, Norway

Dominik Christ
Wikki Ltd., 459 Southbank House, Black Prince Road, London, SE1 7SJ, UK

Summary Numerical simulations of the Sandia flame CHNa and Sydney bluff-body stabilized flame HM1E are reported and the results are compared with the available experimental data. The calculations are based on a new 'rhoEDCFoam' solver, implemented recently in the OpenFOAM toolbox for advanced turbulent combustion modeling, based on compressible URANS/LES formulations. In this study, the calculations are carried out using URANS approach, a standard k-ϵ turbulence model and Eddy Dissipation Concept with detailed chemistry model for the turbulence-chemistry interaction. The syngas (CO/H_2) chemistry diluted by 30% nitrogen of the Sandia flame CHNa is described by a 14 species and 34 elementary reactions mechanism, while CH4/H2 combustion of the Sydney bluff-body flame HM1E is described by the GRI-3.0 mechanism with 325 elementary reactions and 53 species. A robust implicit Runge-Kutta method (RADAU5) is used for integrating stiff ordinary-differential equations to evaluate reaction rates. In general, there is good agreement between present simulations and measurements for both flames, which indicates that the solver is suitable for this type of combustion, provides acceptable accuracy and is ready for further combustion application development.

Introduction

The long-term goal of the present work is to develop a large-eddy simulation (LES) model for high Reynolds number flows of practical interest with further adaptation for turbulent combustion modeling. The core numerical method is based on the OpenFOAM toolbox which was originally developed as a high-end C++ classes library (Field Operation and Manipulation) for a broad range of fluid dynamics applications, but quickly became very popular in industrial engineering as well as in academic research (for example, there are at least two annual international conferences dedicated to the library development and evaluation).

Previously, methodical investigations for several plane turbulent bluff-body flows have been carried out with the goal of validation, verification and understanding of the capabilities of the numerical method using the conventional approach for solution of the unsteady compressible

Reynolds-averaged Navier-Stokes equations (URANS) [24]. These results were analyzed in detail and agreed fairly well with experimental data.

Recently, Lilleberg et al.[22] carried out several turbulent combustion calculations of well-known and detailed flame experiments such as the Sandia Flames D,E [1] and a piloted lean lean-premixed jet burner (PPJB) [7], [8]. Lilleberg and his co-workers [22] used a classical approach for the solution of the steady, compressible Reynolds-averaged Navier-Stokes (RANS) equations, where the turbulence was treated via a standard k-ϵ model [21] and adopted several ways to couple chemical kinetics with the Eddy Dissipation Concept (hereafter EDC) [11], including fast chemistry, local extinction and detailed chemistry approaches. As was expected, the detailed chemistry approach showed the best agreement with the measured data for all cases.

In the present study, we updated the solver application, originally developed by Lilleberg et al.[22], for solving of the unsteady, compressible Reynolds-averaged Navier-Stokes (URANS) equations. The turbulence-chemistry interaction was treated according to the Eddy Dissipation Concept with the detailed chemistry approach. The validation was extended for two benchmark flames: the Sandia Flame CHNa [2] and the Sydney Bluff-Body Flame HM1E [6]. The Sandia Flame CHNa has the advantage of a simple geometry, which enables modelers to focus on the role of the turbulence and kinetic models in the simulations, and minimizes other factors related with the so-called 'discretization errors' [28]. Bluff-body stabilized flames are still a challenging case for turbulent combustion modeling due to the complexity of turbulent flow and finite-rate chemistry, which results in high dimensionality and requires integration of stiff differential equations of chemical kinetics [23].

The paper is divided into four main parts. The first and the second parts of the paper describe the mathematical and numerical modeling, respectively. Then, a general description of the test cases is given. Finally, computational results are presented, results are analyzed and discussed, and conclusions are drawn.

Mathematical modeling

Governing equations

The Favre-averaged (i.e. mass-weighted) equations of mass, momentum and energy conservation for the turbulent compressible flows are:

$$\frac{\partial \bar{\rho}}{\partial t} + \frac{\partial}{\partial x_j}\left(\bar{\rho}\tilde{u}_j\right) = 0 \tag{1}$$

$$\frac{\partial}{\partial t}\left(\bar{\rho}\tilde{u}_j\right) + \frac{\partial}{\partial x_j}\left(\bar{\rho}\tilde{u}_i\tilde{u}_j\right) = -\frac{\partial \bar{p}}{\partial x_i} + \frac{\partial}{\partial x_j}\left(\bar{\tau}_{ij} - \widetilde{\bar{\rho}u_i''u_j''}\right) + \bar{\rho}g_j \tag{2}$$

$$\frac{\partial}{\partial t}\left(\bar{\rho}\tilde{h}\right) + \frac{\partial}{\partial x_j}\left(\bar{\rho}\tilde{h}\tilde{u}_j\right) = \frac{\partial}{\partial x_j}\left(\bar{\rho}\alpha\frac{\partial \tilde{h}}{\partial x_j} - \widetilde{\bar{\rho}u_j''h''}\right) + \bar{S}_h \tag{3}$$

where ρ is the density, u_j is the Cartesian velocity component in the x_j-direction, p is the pressure, τ_{ij} is the viscous stress tensor, h is the total enthalpy, α is the thermal diffusivity, g_j is the gravitation acceleration in the x_j-direction and S_h is the radiation source term. The overbar denotes the Reynolds average, while the tilde denotes Favre average. The turbulence flux $\widetilde{u_j''h''}$ is derived according to the gradient hypothesis

$$-\widetilde{u_j''h''} \approx \frac{\mu_t}{\mathrm{Pr}_t}\frac{\partial \tilde{h}}{\partial x_j} \tag{4}$$

where μ_t is the turbulent viscosity and Pr_t is a turbulent Prandtl number (here $\mathrm{Pr}_t = 0.7$).

For a mixture of N_s species (where $s = 1 \ldots N_s$), transport equation for the mean mass fraction of an individual species Y_s can be defined according to

$$\frac{\partial}{\partial t}\left(\bar{\rho}\tilde{Y}_s\right) + \frac{\partial}{\partial x_j}\left(\bar{\rho}\tilde{Y}_s\tilde{u}_j\right) = \frac{\partial}{\partial x_j}\left(\left(\bar{\rho}D_{m,s} + \frac{\mu_t}{\mathrm{Sc}_t}\right)\frac{\partial \tilde{Y}_s}{\partial x_i}\right) + \bar{\omega}_s,\ s = 1, \ldots, N_s \tag{5}$$

where $D_{m,s}$ is the mass diffusion coefficient for species s in a mixture, Sc_t is the turbulent Schmidt number ($\mathrm{Sc}_t = \mu_t/\rho \mathrm{D}_t$, where D_t is a turbulent diffusivity) and $\bar{\omega}_s$ is the volumetric reaction rate of the species. In the present study, constant dilute approximation was assumed, meaning constant species diffusivity. The turbulent Schmidt number was set to 0.7. Finally, the temperature is related to the density and the pressure by the ideal gas law.

The Reynolds stresses are modeled according to

$$\widetilde{\bar{\rho}u_i''u_j''} = -\mu_t\left(\frac{\partial \tilde{u}_i}{\partial x_j} + \frac{\partial \tilde{u}_j}{\partial x_i} - \frac{2}{3}\delta_{ij}\frac{\partial \tilde{u}_k}{\partial x_k}\right) + \frac{2}{3}\bar{\rho}\tilde{k}\delta_{ij} \tag{6}$$

The standard k-ϵ model [21] is based on the turbulence kinetic energy ($\tilde{k}$) and its dissipation rate ($\tilde{\epsilon}$). The turbulent viscosity is defined here as $\mu_t = C_\mu \bar{\rho}\tilde{k}^2/\tilde{\epsilon}$.

The modeled transport equations are:

$$\frac{\partial}{\partial t}\left(\bar{\rho}\tilde{k}\right) + \frac{\partial}{\partial x_j}\left(\bar{\rho}\tilde{k}\tilde{u}_j\right) = \frac{\partial}{\partial x_j}\left(\left(\mu + \frac{\mu_t}{\sigma_k}\right)\frac{\partial \tilde{k}}{\partial x_j}\right) + G - \bar{\rho}\tilde{\epsilon} \tag{7}$$

$$\frac{\partial}{\partial t}\left(\bar{\rho}\tilde{\epsilon}\right) + \frac{\partial}{\partial x_j}\left(\bar{\rho}\tilde{\epsilon}\tilde{u}_j\right) = \frac{\partial}{\partial x_j}\left(\left(\mu + \frac{\mu_t}{\sigma_\epsilon}\right)\frac{\partial \tilde{\epsilon}}{\partial x_j}\right) + C_{\epsilon 1}\frac{\tilde{\epsilon}}{\tilde{k}}G - C_{\epsilon 2}\bar{\rho}\frac{\tilde{\epsilon}^2}{\tilde{k}} \tag{8}$$

where μ is the molecular viscosity, and the rate of turbulence kinetic energy production G is given as

$$G = -\widetilde{\bar{\rho}u_i''u_j''}\frac{\partial \tilde{u}_i}{\partial x_j} \tag{9}$$

The standard values [21] were used for the model constants C_μ,$C_{\epsilon 1}$, $C_{\epsilon 2}$, σ_k and σ_ϵ.

EDC for turbulent combustion

The Eddy Dissipation Concept for turbulent combustion [26],[11] is based on the energy cascade model. Strictly following Geurts [14], a turbulent flow (according to the ideas of Richardson [32]) can be considered as consisting of eddies with various characteristic length-scales. The smaller, more localized eddies are exposed to the strain rate field arising from the larger eddies. There is an average energy flux from the larger to the smaller eddies, which is called the energy cascade. The energy cascade is fed by turbulence production, and energy is finally dissipated by viscous effects at sufficiently small scales. The EDC assumes that molecular mixing and chemical reactions occur on the smaller dissipative eddies, which are close to the Kolmogorov length scales and are termed 'fine structures'. The characteristic length L^* and velocity u^* scales of the fine structures are of the same order of magnitude as Kolmogorov scales and can be expressed as

$$L^* = \frac{2}{3}\left(\frac{3C_{D2}^3}{C_{D1}^2}\right)^{1/4}\left(\frac{\nu^3}{\tilde{\epsilon}}\right)^{1/4} \tag{10}$$

$$u^* = \left(\frac{C_{D2}}{3C_{D1}^2}\right)^{1/4}(\nu\tilde{\epsilon})^{1/4} \tag{11}$$

where $C_{D1} = 0.134$ and $C_{D2} = 0.5$ [11]. RANS-based EDC assumes that the full cascade takes place at each numerical cell, and the connection between the fine structure and the larger eddies is achieved through the cascade. Thus, characteristics of the large eddies such as velocity u' are evaluated using the turbulence model (in the present case, the standard $k - \epsilon$ model).

In the model expressed below, different superscripts refer to states inside fine structures (*), surroundings ($\circ$) and mean values of the computational cell ($\sim$).

The ratio between the mass in the fine structures and the total mass is postulated as

$$\gamma^* = \left(\frac{u^*}{u'}\right)^3 = \left(\frac{3C_{D2}}{4C_{D1}^2}\right)^{1/4} \left(\frac{\nu\tilde{\epsilon}}{\tilde{k}^2}\right)^{1/4} \tag{12}$$

The mass exchange between the fine structures and the surroundings, divided by the mass of the fine structures, is defined as

$$\dot{m}^* = 2\frac{u^*}{L^*} = \left(\frac{3}{C_{D2}}\right)^{1/2} \left(\frac{\tilde{\epsilon}}{\nu}\right)^{1/2} \tag{13}$$

The mass exchange between the fine structures and the surroundings, divided by the total mass, is calculated according to

$$\dot{m} = \gamma^* \dot{m}^* \tag{14}$$

The mass-averaged mean reaction rate for the sth specie is given as

$$-\bar{\omega}_s = \frac{\bar{\rho}\dot{m}\chi}{1 - \gamma^*\chi} \left(\tilde{Y}_s - Y_s^*\right), \; s = 1, \ldots, N_s \tag{15}$$

and the relationship between the mass-averaged mean state, fine-structure state and surrounding state is expressed as

$$\tilde{\Psi} = \gamma^*\chi\Psi^* + (1 - \gamma^*\chi)\Psi^\circ \tag{16}$$

Here, χ is the reacting fraction of the fine structures, which can depend on probability of co-existence of the reactants, degree of heating and a limiter to the reaction due to lack of reactants. In the present study, $\chi = 1$, as suggested by Gran and Magnussen [15]. The mean mass fraction $\tilde{Y}_s$ for species s is calculated from solving the species mass transport equation for each individual species. The fine-structure mass fraction Y_s^* is computed through the detailed chemistry approach.

EDC detailed chemistry approach

Finite-rate chemical kinetics are taken into account by treating the fine structures as constant pressure and adiabatic homogeneous reactors. Thus, the fine structures mass fractions values Y_s^* can be calculated a system of ordinary differential equations (ODE) describing a Perfectly Stirred Reactor (PSR) concept [15],

$$\frac{dh^*}{dt} = 0 \tag{17}$$

$$\frac{dp^*}{dt} = 0 \tag{18}$$

$$\frac{dY_s^*}{dt} = \frac{\omega_k^*}{\rho^*} + \frac{1}{\tau^*}\left(Y_s^\circ - Y_s^*\right), \; s = 1, \ldots, N_s \tag{19}$$

The reaction rate ω_k^* is evaluated from a chemical kinetics mechanism, and Y_s° is the mass fraction of the inflow stream to the reactor. In the present study, it was assumed adiabatic and isobaric PSRs, and time derivatives for h^* and p^* were not included in calculations. Also, it was assumed that PSRs are at steady state [15], meaning that the steady-state solution of the Eq.19 is achieved by integrating it in time to steady state.

It is worth noticing, that the residence or mixing time scale τ^* was evaluated using the molecular viscosity and the dissipation rate

$$\tau^* = \frac{1}{\dot{m}^*} \tag{20}$$

The chemical kinetic mechanism GRI-3.0 [3] was used for modeling the Sydney Flame HM1E. This mechanism has been specially designed for combustion of natural gas with air. The mechanism contains 325 elementary reactions and 53 species.

Another kinetic model, consisting of 34 elementary reactions and 14 species [10], was used for syngas combustion (Sandia Flame CHNa). This mechanism has been developed specially for syngas combustion applications by Frassoldati, Faravelli and Ranzi [10] and validated against a set of experimental measurements (including plug flow reactor, PSR, shock tubes and ignition delay times, laminar flame speed, and ignition in a counter-flow flame). We assigned the acronym FFR to this mechanism, which is formed by the first letters of the developers's last names [10] in the spirit of Marzouk and Huckaby [28].

Modeling radiation

In the present study, the radiation was modeled by the P1-approximation, which is the simplest form of the more generalized P-N method (or spherical harmonics) [4]. The gas radiation properties were established from the concentrations of CO_2 and H_2O, which were available from the combustion calculation. A weighted-sum of gray gases (WSGG) method was employed for the radiation properties calculations [13]. The model coefficients were taken from Smith et al. [34].

Brief description of numerics

Core numerical method

The OpenFOAM code [36] was used for the numerical simulations. The new solver rhoEDCFOAM was implemented through the modification for the build-in application rhoPimpleFoam for the the compressible URANS modeling based on the finite-volume (FVM) method [14] and the predictor-corrector PIMPLE procedure, which is a merge of the PISO (pressure implicit with splitting of operators) and SIMPLEC algorithms [18],[31]. The preconditioned (bi-) conjugate gradient method [16] with incomplete-Cholesky preconditioner (ICCG) by Jacobs [19] was used for solving linear systems with a local accuracy of 10^{-7} for all dependent variables at each time step.

The numerical method had second-order accuracy in space and time. The linear-upwind interpolation scheme (sometimes referred to as the 'second-order upwind' scheme), with the face value calculated by linear extrapolation from the two upwind cell values [35], was applied for all convective terms approximation. Linear (second-order central differences) interpolation was used to calculate the diffusion terms. A second-order implicit Euler method (BDF-2 [14]) was used for time integration together with the dynamic adjustable time stepping technique to guarantee a local Courant number less than 0.4.

The calculation of the mean species reaction rate $\bar{\omega}_s$ requires the integration of Eq.19 for each cell in the domain. For this purpose, the robust RADAUS5 algorithm [12] was used. The

RADAUS5 algorithm is designed for the solving stiff ODE systems and applies a 5th order accurate implicit Runge-Kutta method based on the Radau quadrature formula. The relative tolerance, absolute tolerance and maximum number of iterations to meet the target accuracy were set to 5×10^{-5}, 1×10^{-5} and 10^7, respectively.

Boundary and initial conditions

All problems were solved assuming symmetry about the centerline. For all cases, a computational domain was designed as a sector of 5° with imposed periodic boundary conditions and included pre-inlet pipes for the fuel-jet in order to obtain fully-developed turbulent velocity profiles. A uniform velocity profile was specified for the air co-flow. All radial and circumferential velocity components were set to be zero. The inflow temperatures were set based on the experimental settings. The exit pressure was specified to 10^5 Pa at the outlet, and zero-gradient pressure was imposed at the inlet boundaries. The co-flow inner and outer boundaries were treated as iso-thermal perfect-slip walls. A non-slipping condition for velocity was applied for other walls. Wall-functions were applied for k, ϵ and μ_t. The temperature at the walls was calculated according to the zero gradient boundary condition. The fuel jet, pilot and co-flow compositions were specified in terms of the species mass fractions calculated from the experimental data. Marshak's boundary conditions, based on solutions of Legendre polynomials of odd order [27], were adopted for radiative heat flux calculations.

It is worth noticing, that calculations of reacting flows with EDC and the detailed chemistry approach are very sensitive to initial conditions with respect to stability [22]. In the present study, the cold-flow solution was used as a starting value. To initiate the combustion process, ignition of the mixture was modeled as an artificial spark, by patching a hot temperature into a region of the computational domain that contains flammable fuel/oxidant concentrations.

Grid dependence study

The present results were obtained using two sets of grids for each of the flames: a low-resolution grid and a high resolution grid. The high-resolution grids were created by simple refinement of the low-resolution grids by a factor of 2×2 in the axial and radial directions. The details of the high-resolution grids are provided in the next section. In general, the differences between the two sets of grids were insignificant for both flames, and it was therefore concluded that the high-resolution grids were sufficiently accurate for testing of the mathematical models on the chosen flames.

Data sampling

Since unsteady Navier-Stokes equations were considered, data sampling was used in order to obtain time independent results. Fig. 1 shows some jet pulsations for the Sandia flame CHNa and recirculation zone oscillations for the Sydney bluff-body flame HM1E. Since the compressible formulation with the stability condition CFL < 0.4 and a high resolution grid were used, the typical values of integration time step did not exceed 5×10^{-6} s. The resolution of the shedding cycle varied in a range of several thousands time steps. Time-averaging was done for 10 characteristic shedding cycles for each flame to achieve statistically stationary flow field. Hereafter, the time-averaging operator is denoted by $\langle\rangle$.

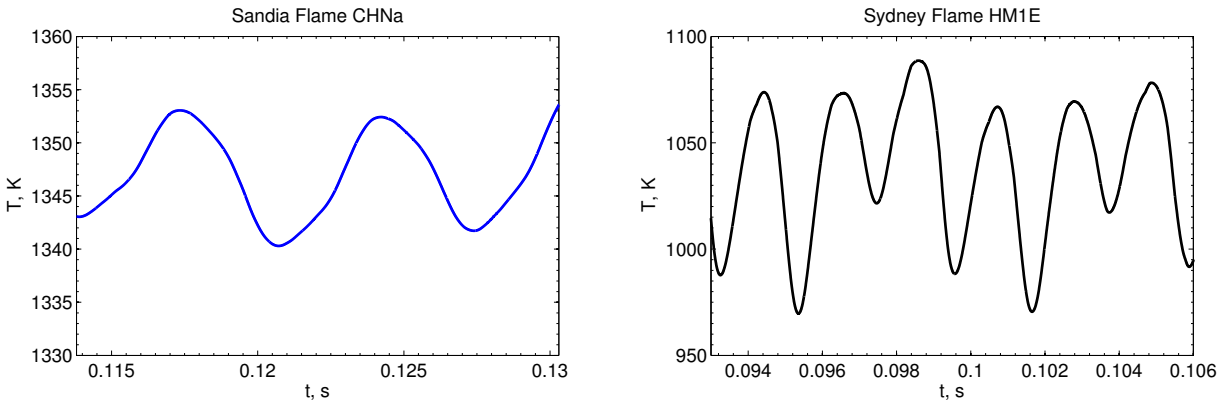

Figure 1: Time history of the temperature for the Sandia CHNa flame and the Sydney HM1E flame. The probes location were at $x = 0.3$, $y = 0.0065$ and $x = 0.048$, $y = 0.006$ for CHNa and HM1E flames, respectively.

Test case descriptions

Sandia Flame CHNa

The simple turbulent non-premixed syngas $40\%\text{CO}/30\%\text{H}_2/30\%\text{N}_2$ (by volume) flame, examined experimentally by Sandia National Laboratories (scalar measurements) and the Swiss Federal Institute of Technology – ETH (LDA measurements) [2] was examined. The burner tube had an inner diameter $D = 4.58$ mm and an outer diameter of 6.34 mm. The tube had a thickness of only 0.88 mm, however this was sufficient for flame stabilization via a small recirculation zone. The fuel jet Reynolds number was $\text{Re}_j = U_j D/\nu_j = 16.7 \times 10^3$, where $U_j = 76$ m/s was the fuel jet velocity and $\nu_j = 2.083 \times 10^{-5}$ m^2/s was the kinematic viscosity. The jet temperature was 292 K. The co-flow stream had a velocity of 0.7 m/s, a temperature of 290 K and a 1.2% mole fraction of water vapor. Experimental data include axial and radial profiles of mean and root-mean-square (rms) values of temperatures and major species mass fractions as well as velocities and Reynolds stresses.

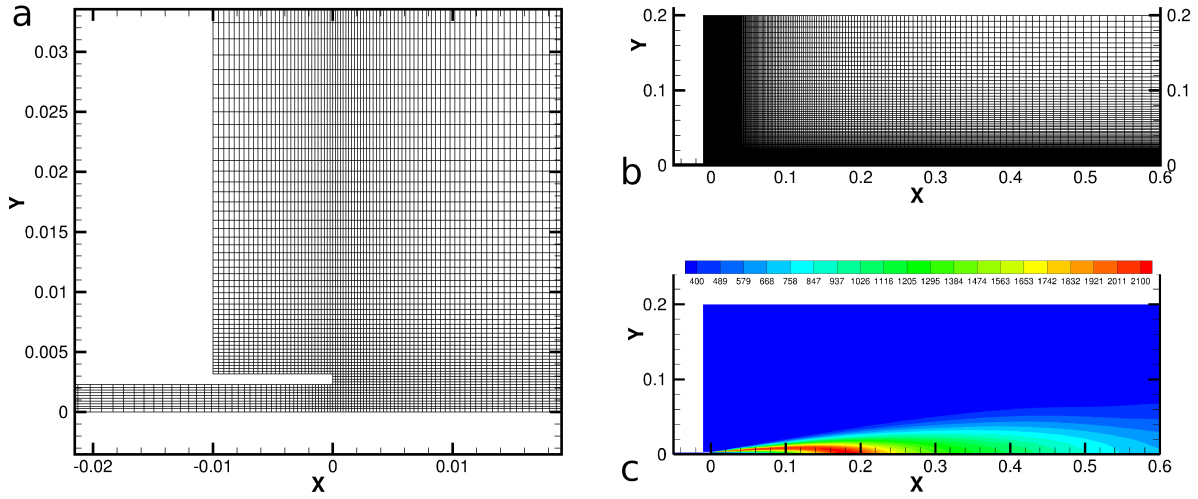

Figure 2: Details of the grid near the inlet (a) and a general view of the computational domain (b) for the Sandia CHNa flame; 20 iso-contours of mean temperature (c) in a range of 400-2100 K.

Some details of the grid and computational domain are shown in Fig. 2. The axial and radial dimensions of the computational domain after the burner exit were set to 600 mm ($131 \times D$) and 200 mm ($43.627 \times D$), respectively. The number of cells along the axial direction was 230 and the number of cells in the radial direction was 100. The length of the pre-inlet fuel pipe was 50 mm ($10.917 \times D$) and contained 90 cells. The grid expansion factors were 1.09 and 1.14 in the axial and radial (from the burner tube) directions, respectively. There were 10 cells along the inner radius of the fuel jet and 4 cells along the burner tube wall with uniform distribution in the radial direction.

Several studies of the CHNa flame are available in the literature. Cuoci et al. [5] have modeled numerically the CHNa and CHNb flames using RANS with several different approaches for the turbulence-chemistry interaction, such as the Eddy Dissipation Concept [25],[11] and the steady laminar flamelets model [9]. They reported that EDC (coupled with the FFR kinetic scheme) provided the best results.

In contrast to Cuoci et al. [5], Marzouk and Huckaby [28] have studied the CHNa flame using the conventional URANS approach. They adopted Chalmer's partially stirred reactor model (PaSR) [33] for the turbulence-chemistry interaction and investigated eight chemical kinetic mechanisms (including FFR model). However, Marzouk and Huckaby obtained the most accurate predictions with a simple 3 step/5-species kinetic model.

Sydney Bluff-Body Flame HM1E

The Sydney bluff-body Flame HM1E configuration consists of a rotationally symmetric bluff-body nozzle (diameter $D_B = 50$ mm) which is placed in a square duct of 130 mm width. Gas is fed through a centered pipe (diameter of 3.6 mm) at a bulk jet velocity of $U_j = 108$ m/s at ambient conditions with a jet Reynolds number, $Re_j = 15.8 \times 10^3$. The secondary air stream between the duct and the burner nozzle is fixed at 35 m/s. All velocities and velocity fluctuations were measured through Laser Doppler velocimetry (LDV), and scalar measurements were carried out using the Raman/Rayleigh/LIF techniques[6].

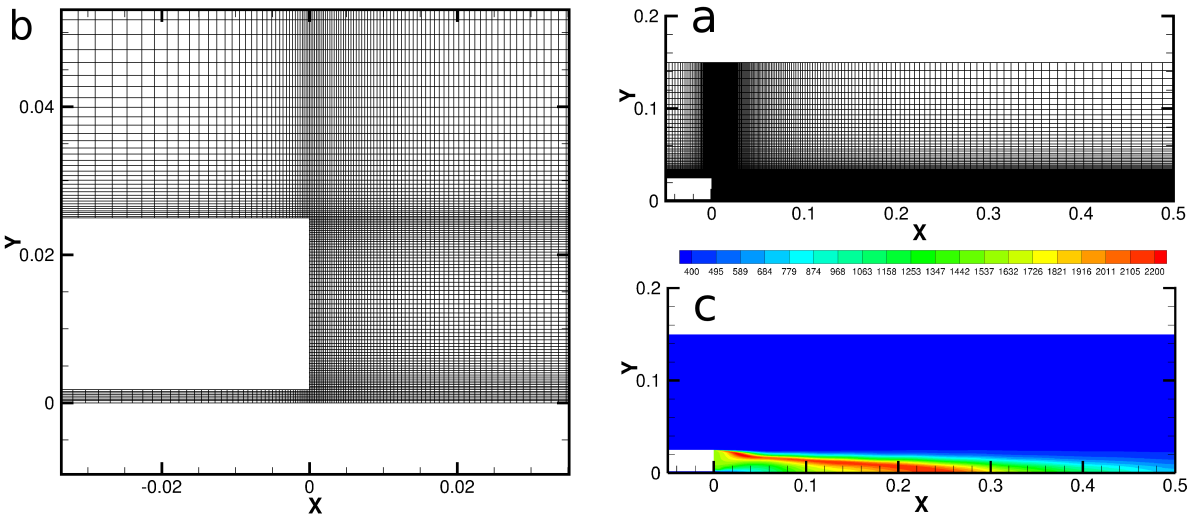

Figure 3: General view of the computational domain (a) and details of the grid near the inlet (b) and for the Sydney bluff-body HM1E flame; 20 iso-contours of mean temperature (c) in a range of 400-2100 K.

Some details of the grid and computational domain are shown in Fig. 3. The axial and radial dimensions of the computational domain after the bluff-body were set to 500 mm ($20 \times D_B$)

and 150 mm ($6 \times D_B$), respectively. The number of cells along the axial direction was 170, and the number of cells in the radial direction was 120. The grid expansion factors were 1.1 and 1.12 (from the bluff-body) in the axial and radial directions, respectively. The length of the pre-inlets for the fuel pipe and co-flow was 50 mm ($2 \times D_B$) and contained 50 cells. The number of cells (in the radial direction) located in the jet, bluff-body and co-flow was 8, 60 and 52, respectively. The inner radius of the fuel jet had a uniform distribution of cells in the radial direction, while the bluff-body had bi-exponentiation distribution of nodes from the mid to the fuel jet and co-flow.

Several researchers have performed simulations of the Sydney bluff-body flames with different turbulence and combustion models. Liu et al. [23] provided a comprehensive overview of previous works. However, it is worth noticing that there is a lack of published data related to use of EDC, coupled with a detailed chemistry approach.

Results

Sandia Flame CHNa

Fig. 4 compares the profile of the axial velocity, temperature and species mass fractions obtained in the present simulations with experimental data from Barlow et al. [2]. In general, agreement is very satisfactory, even though the predicted peak axial temperature was over-estimated. Several reasons may cause such over-predicted temperature. According to the study by Hewson and Kerstein [17], two possible reasons such as neglecting of the radiative heat losses and under-predicting the dissipation rate were responsible for the temperature over-prediction ($50 - 150$ K). However, Cuoci et al. [5] reported that thermal radiation affects the peak temperature only by about $30 - 40$ K. Moreover, they investigated in detail the effect of the grid density and the applied numerical schemes and concluded that the peak temperature was nearly insensitive to these factors. Cuoci et al. [5] speculated that the most important factor was the turbulence model used. Indeed, different turbulence models affect the jet penetration and the scalar dissipation rate and turbulent mixing. Cuoci et al. [5] used the standard k-ϵ model with a corrected $C_{\epsilon 1}$ constant (according to McGuirk and Rodi [29]) in their study and did not get significant temperature over-prediction. It is evident as well, that any model overestimation of the flame temperature affect the prediction of the species. Thus, it is observed that the reactions occurred too much upstream, hence releasing the thermal energy and producing $\langle Y_{H2O} \rangle$ and $\langle Y_{CO2} \rangle$. However, the match between other measured and predicted species ($\langle Y_{N2} \rangle$, $\langle Y_{O2} \rangle$, $\langle Y_{H2} \rangle$, $\langle Y_{CO} \rangle$, $\langle Y_{OH} \rangle$) were quite good.

A detailed comparison of the radial profiles at the axial distances $x/D = 20$ and $x/D = 40$ are presented in Fig. 5 and Fig. 6, respectively. The predicted radial profile of the mean axial velocity at 20 jet diameters downstream the nozzle exit was in good agreement with the measurements. The mean axial velocity decayed rapidly from about 80 m/s at the centerline to the co-flow stream velocity.

However, the jet spreading was not surprisingly over-predicted, since the standard k-ϵ model without correction was applied. The calculated mean species $\langle Y_{O2} \rangle$, $\langle Y_{CO2} \rangle$ and $\langle Y_{H2O} \rangle$ had the similar behavior as the mean temperature. Other species $\langle Y_{N2} \rangle$, $\langle Y_{H2} \rangle$, $\langle Y_{CO} \rangle$, $\langle Y_{OH} \rangle$ were in reasonable agreement with the experiment.

Based on the comparison of the predicted and measured radial profiles of the mean axial velocity at $x/D = 40$ downstream the nozzle exit, it is evident that the present calculations slightly under-estimated the decay of the jet (which is also the consequence of using a not corrected k-ϵ

model). Keeping this fact in mind, agreement between computed and measured mixture components was reasonable, except $\langle Y_{H2} \rangle$, which was under-predicted near the centerline, indicating high oxidation rates at the axial distance.

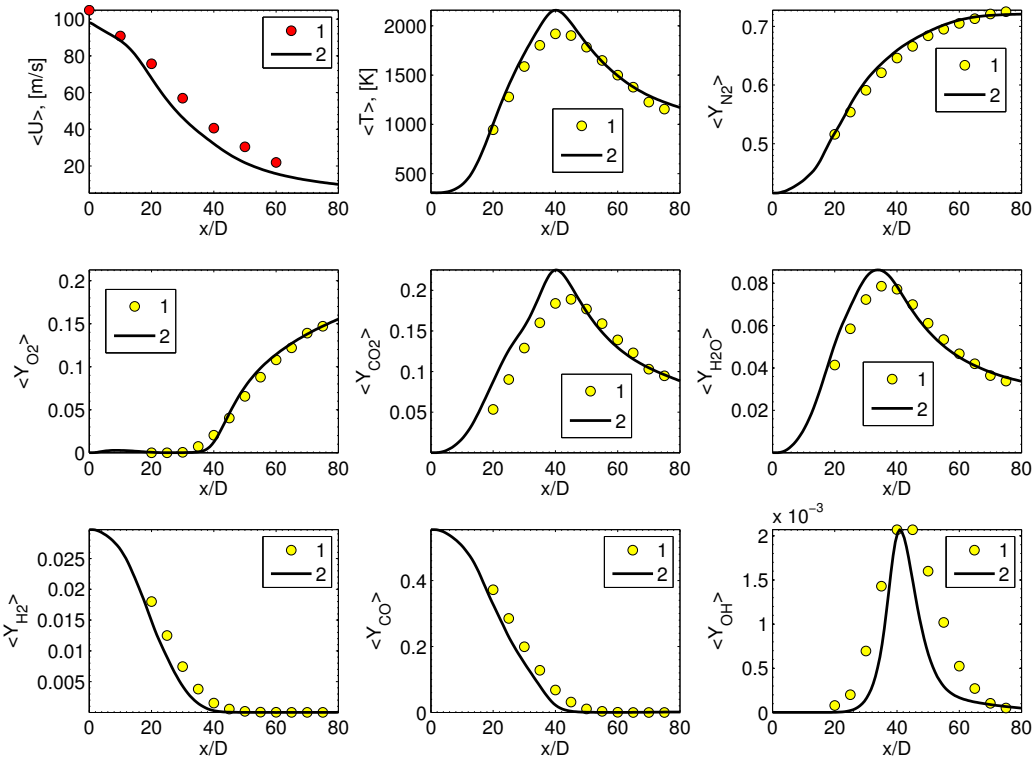

Figure 4: Mean axial velocity, mean temperature and mean composition profiles along the axis for the Sandia flame CHNa: 1 - experiment, 2 - present calculations.

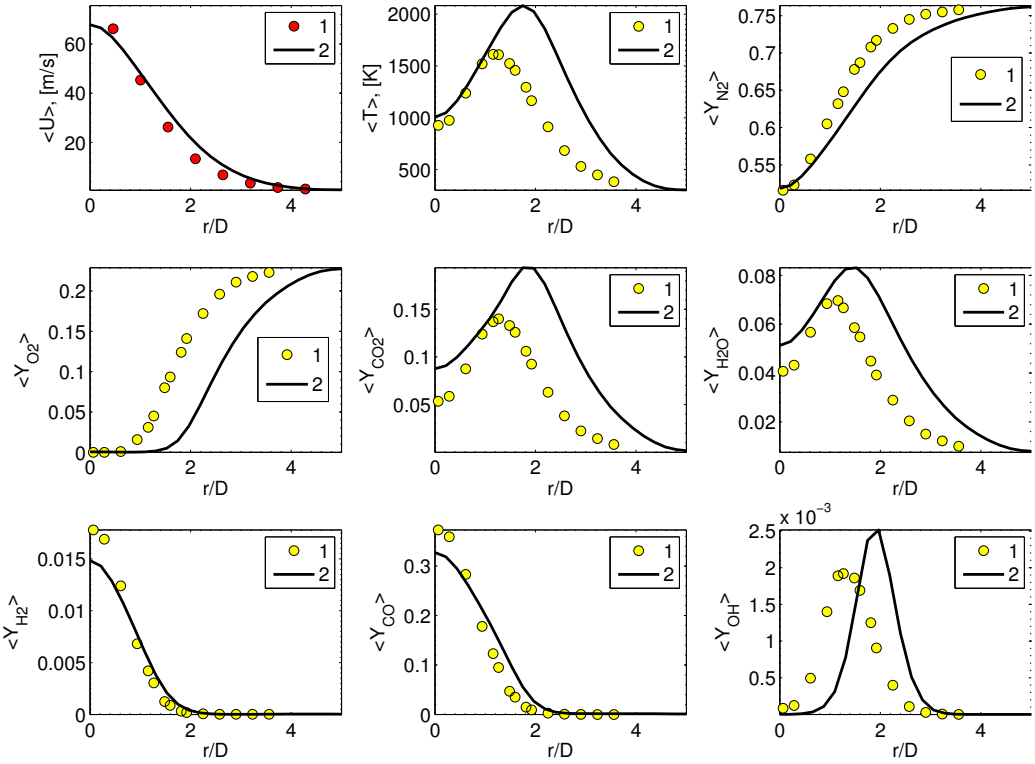

Figure 5: Mean axial velocity, mean temperature and mean composition radial profiles at $x/D = 20$ for the Sandia flame CHNa: 1 - experiment, 2 - present calculations.

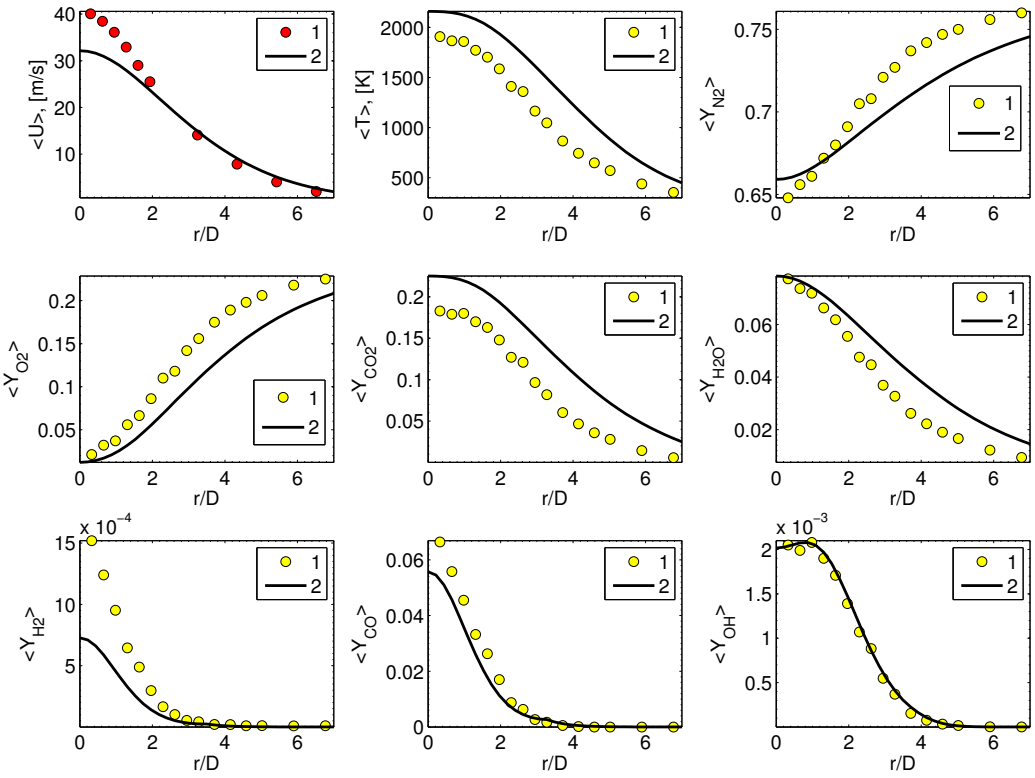

Figure 6: Mean axial velocity, mean temperature and mean composition radial profiles at $x/D = 40$ for the Sandia flame CHNa: 1 - experiment, 2 - present calculations.

Sydney Bluff-Body Flame HM1E

Predicted radial profiles of the mean velocities are compared to experimental data in Figs. 7-8. Generally, the agreement between the present data and the measurements was good at upstream locations (up to $x/D = 1.4D_B$), which were within the recirculation zone. Some discrepancies were observed further downstream, starting from about $x/D = 2.8D_B$. Both the shape and the peak values of the radial profiles of the mean axial $\langle U \rangle$ and radial $\langle V \rangle$ velocities were well captured within the recirculation zone. The jet penetration depth, the spreading and the positions of the two shear layers were predicted quite well. It is interesting to note, that the axial velocity decayed too slowly at the symmetry axis compared to experimental data. This is not in agreement with the predictions by Yan et al. [37] and Liu et al. [23], who reported the contrary behavior of the mean axial velocity at the symmetry axis. It is possible that the use of the unsteady algorithm in the present calculations may be one of the explanations for these discrepancies. The magnitudes of mean radial velocities were significantly smaller than the magnitudes of the mean axial profiles (approximately by one order of magnitude). However, the agreement between the present results and the measured data was reasonable for all of the radial profiles.

Streamline pattern is shown in Fig. 9. The flame was stabilized by the recirculation zone behind the bluff-body which traps hot gases. By definition, the recirculation length ($\langle L_r \rangle$) corresponds to the distance between the base of the bluff-body and the sign change of the centerline mean axial velocity. The calculated recirculation zone length was $1.06D_B$. Precise experimental data for $\langle L_r \rangle$ were not available, however its value could be bounded between between $x/D = 1.4$ and $x/D = 1.8$, as seen in Fig. 7. It is seen, that $\langle L_r \rangle$ was under-predicted in the present calculations. However, this result was consistent with the predictions by Yan et al. [37], who also used the standard $k - \epsilon$ model in their simulations of the Sydney bluff-body flames.

Figs. 10 - 12 compare time-averaged scalar fields at three axial locations. In general, temperature profiles matched the experimental data well. The spurious well-formed peak in the predicted temperature profiles in the shear layer between the co-flow and the recirculation zone may be explained by the artificial boundary conditions. Indeed, we applied the perfect-slip conditions for velocity at the outer edge of bluff-body, which occurred not very accurate and led to the serious over-prediction of the temperature in the shear layer. The radial profiles of $\langle Y_{O2} \rangle$, $\langle Y_{N2} \rangle$, $\langle Y_{H2} \rangle$ and $\langle Y_{H2O} \rangle$ matched well the experimental data. There were some discrepancies for $\langle Y_{CO2} \rangle$. These discrepancies could be explained by the temperature behavior in the shear layer. The agreement for $\langle Y_{CO} \rangle$, $\langle Y_{OH} \rangle$ and $\langle Y_{NO} \rangle$ was quite good inside the recirculation bubble, and less satisfactory at the axial location of $x/D = 1.3$, with the calculations showing the correct trends, except the area of shear layer, where, as it was discussed, the temperature was clearly over-predicted.

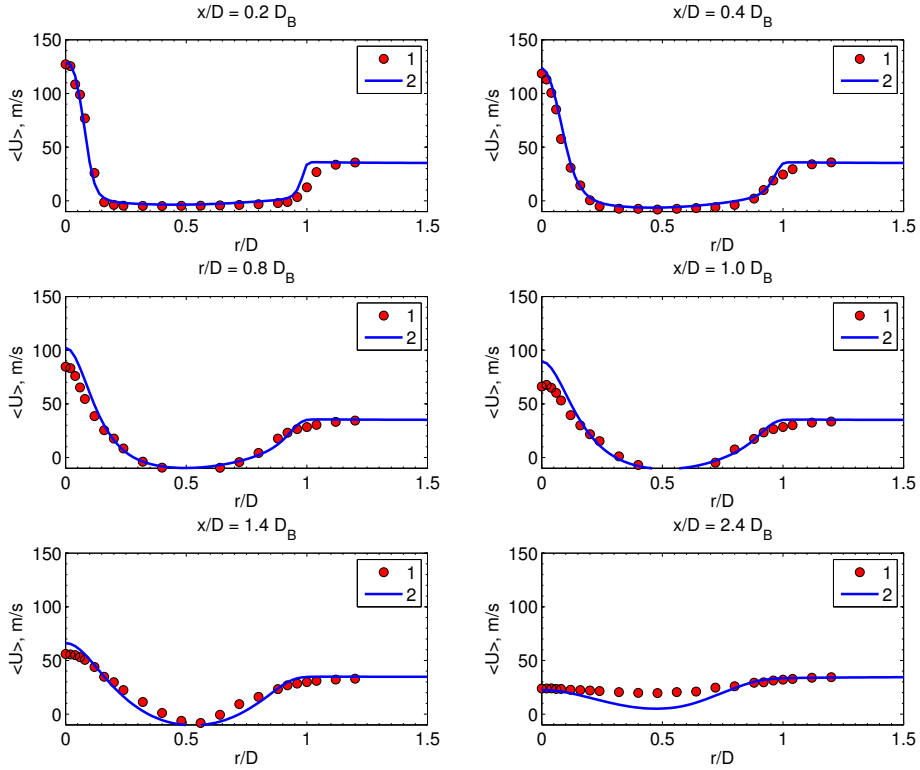

Figure 7: Radial profiles of the mean axial velocity for the Sydney bluff-body flame HM1E: 1 - experiment, 2 - present calculations.

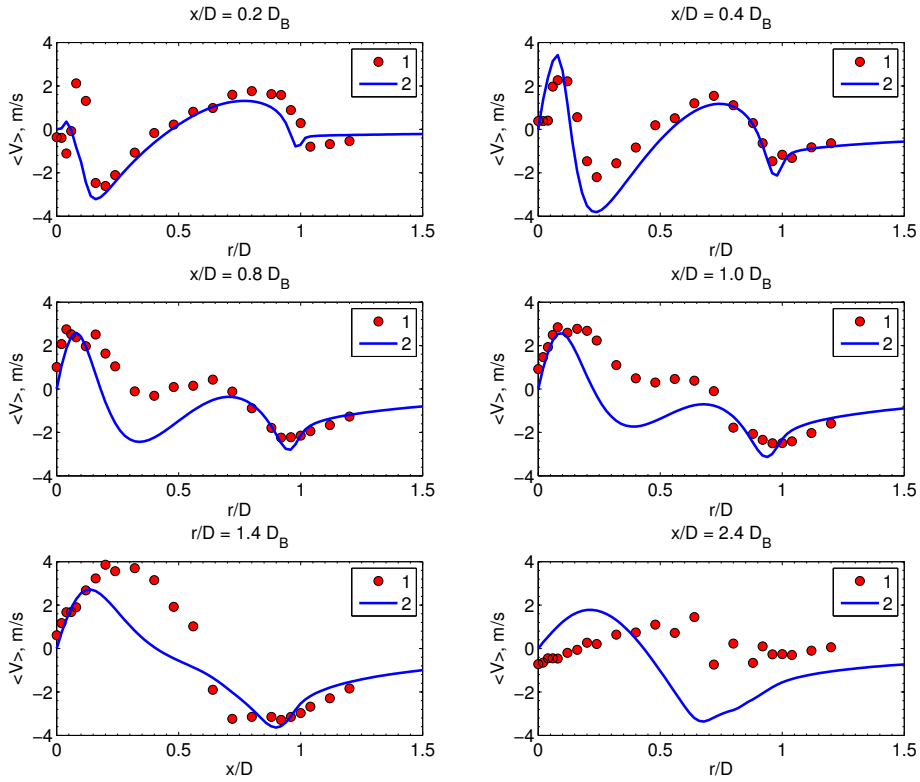

Figure 8: Radial profiles of the mean radial velocity for the Sydney bluff-body flame HM1E: 1 - experiment, 2 - present calculations.

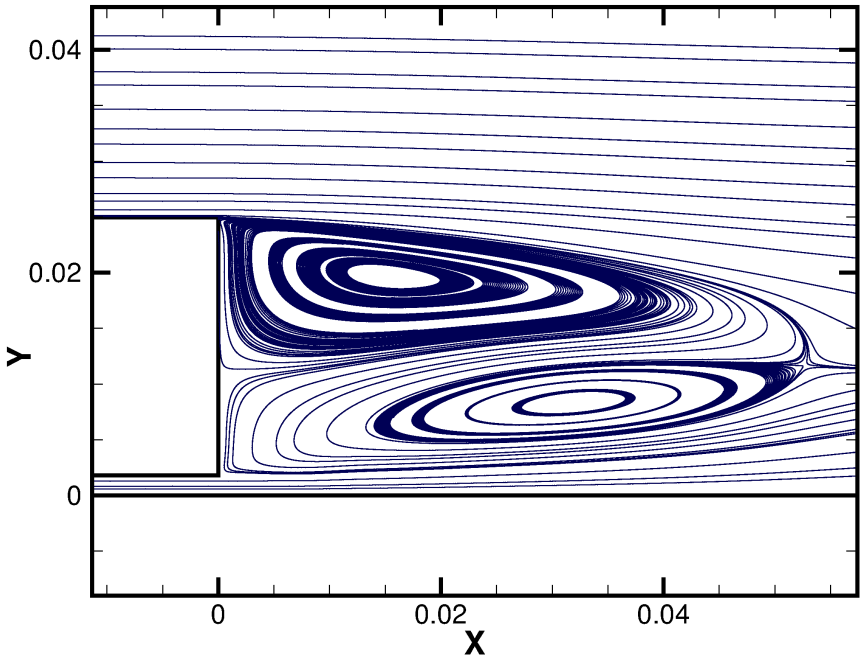

Figure 9: Time-averaged streamlines for the Sydney bluff-body flame HM1E.

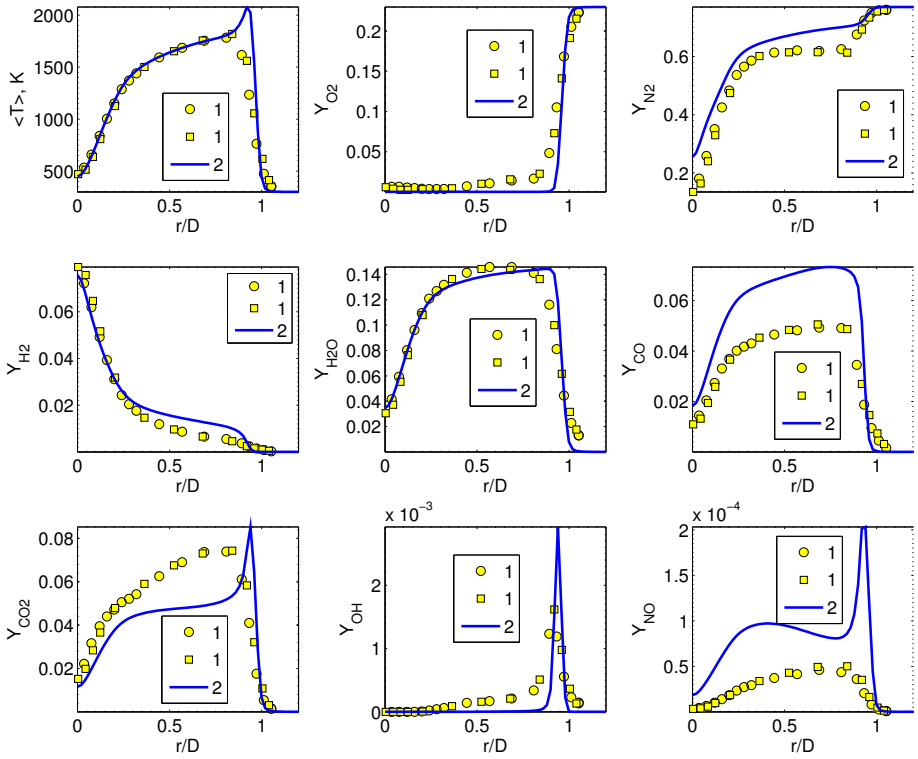

Figure 10: Radial profiles of the mean temperature and compositions at $x/D_B = 0.6$ for the Sydney bluff-body flame HM1E: 1 - experiment, 2 - present calculations.

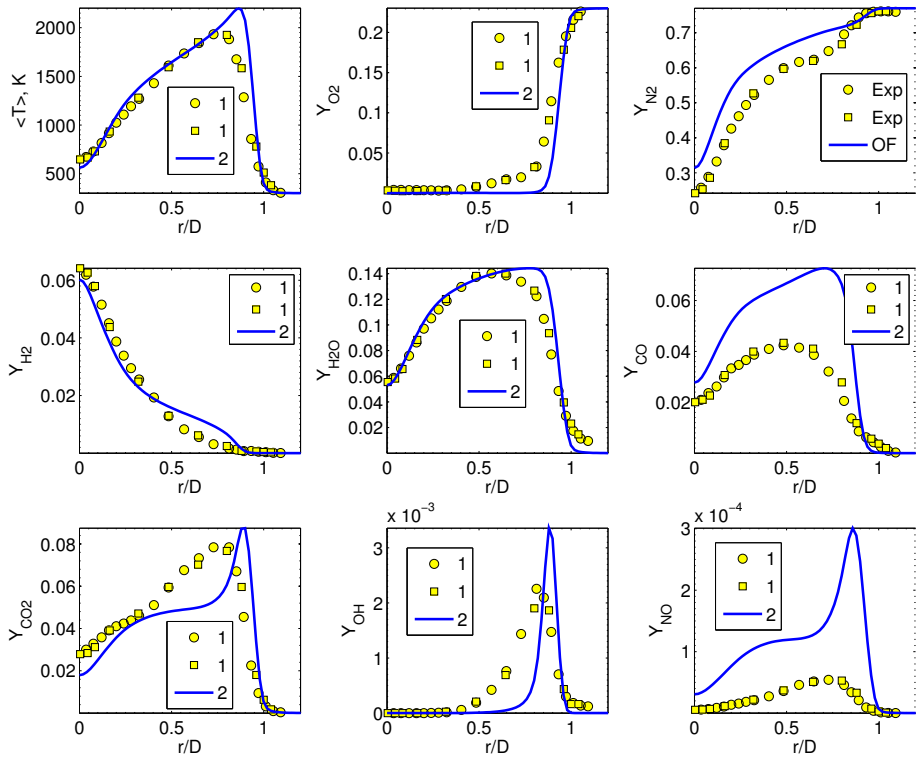

Figure 11: Radial profiles of the mean temperature and compositions at $x/D_B = 0.9$ for the Sydney bluff-body flame HM1E: 1 - experiment, 2 - present calculations.

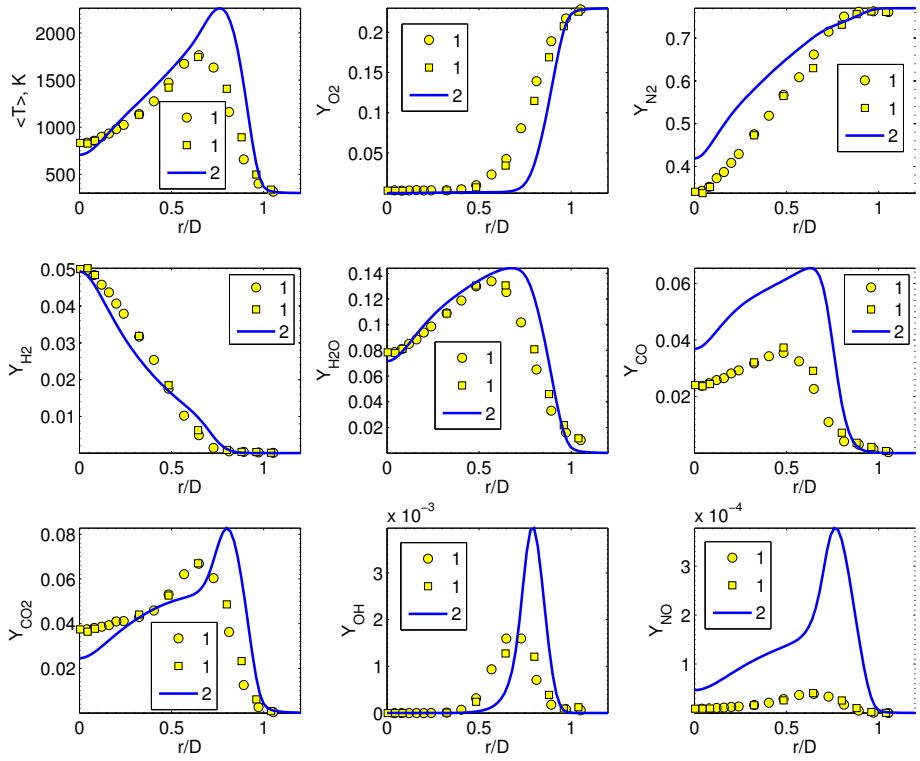

Figure 12: Radial profiles of the mean temperature and compositions at $x/D_B = 1.3$ for the Sydney bluff-body flame HM1E: 1 - experiment, 2 - present calculations.

Discussion

Numerical predictions of the Sandia CHNa flame and Sydney bluff-body HM1E flame has been carried out. In general, in spite of some discrepancies, relatively good agreement was achieved for both flames in terms of velocity fields, temperature and the species concentrations.

In general, the disagreement between experimental data and numerical results is determined by two groups of errors (apart from experimental errors): (1) 'model' errors due to inadequate assumptions made in selecting one turbulence model or another and (2) 'discretization' errors caused by the inadequate resolution of the employed computational grids and computational methods. Whereas the errors of the first group are assumed to be 'systematic' under certain assumptions, e.g., for a fixed computational methodology, 'discretization' errors are controlled by the method of adaptation (increase in the resolution) of a computational grid.

From the 'model' error point of view the following critical remark should be done. Here, the turbulence-chemistry interaction was modeled using EDC with detailed chemistry, while the standard k-ϵ model was used for the turbulence. Choosing appropriate models for turbulence and chemistry would play an important role for modeling of the turbulent reacting flows. In the present study we did not investigate the influence of chemistry, since the detailed mechanisms were applied for both flames and since it was out of the scope of the present work. However, as it was discussed, the peak temperature for the Sandia flame CHNa was over-predicted in the present simulations, and one of the possible reasons for this may be caused in the chemistry kinetics. Moreover, the standard k-ϵ model without any modifications was applied. We did not perform any sensitivity study with respect to the turbulence modeling. However, the standard k-ϵ model over-predicts spreading and diffusion for round-jet flows [29]. A change of model constant values is a common remedy to reduce spreading/diffusion and increase the predictive capabilities of the model.

From the 'discretization' error point of view, two sets of grids were used in the present study to check the mesh-error influence. It is worth noticing, that in spite of the fact that calculations were carried out in 2 dimensions, it was required approximately $3-5$ weeks to get statistically-converged solutions on the high-resolution grids using one node (16 cores in parallel) on the 'Vilje' high-performance facility (www.notur.no). The main reason for this is the finite-rate chemistry. This shows that turbulent flow simulations with detailed chemistry are resource expensive even for $2D$ problems. The present calculations did not reveal significant deviations between the solutions obtained on the low-resolution (not presented here) and the high-resolution grids. The resolution of the applied grids was therefore concluded to be sufficient for the scope of the present work.

The influence of the 'temporal discretization' errors was not analyzed in the present study. Usually the spatial discretization error effect is larger than the error arising from time integration [14]. It could be shown that in case of fully developed turbulent flows, existed small time and space scales are simply advected by the most energetic eddies [14]. This argument yields an accuracy time-scale similar to the CFL criterion. Thus, in all present calculations, the stability condition CFL < 0.4 was employed, which guaranteed that the actual time step was close to accuracy time step.

Concluding remarks

The Eddy Dissipation Concept combined with a detailed chemistry approach was applied to the Sandia CHNa flame and the Sydney bluff-body HM1E flame. The syngas (CO/H_2) chemistry of the Sandia flame CHNa was described by a 14 species and 34 elementary reactions

mechanism, while CH4/H2 combustion of the Sydney bluff-body flame HM1E was described by the GRI-3.0 mechanism. A robust implicit Runge-Kutta method (RADAU5) was used for integrating stiff ordinary-differential equations to evaluate reaction rates. Statistically stationary results were obtained and compared with the available experimental data in detail. In general, there was relatively good agreement between present simulations and measurements for both flames. Here, the standard k-ϵ model has been used to model the turbulent flow and it would be worthwhile to investigate the performance of other turbulence models in future work. It is believed that one of the main reasons for the observed discrepancies between the predictions and experimental data is the round-jet anomaly of the k-ϵ turbulence model.

Overall, the present results (together with previously obtained results) give a good indication on the adequacy and accuracy of the implemented solver and its readiness for further combustion application development.

Acknowledgment

This work was conducted as a part of the CenBio Center for environmentally-friendly energy. We are very appreciated to the Norwegian Meta center for Computational Science (NOTUR) for providing the uninterrupted HPC computational resources and the useful technical support.

References

[1] Barlow, R. S. and Frank, J. H., Effects of turbulence on species mass fractions in methane/air jet flames, Proc. Combust. Inst. 27, 1087–1095 (1998)

[2] Barlow, R. S., Fiechtner, G. J., Carter, C. D., and Chen, J.-Y., Experiments on the Scalar Structure of Turbulent CO/H2/N2 Jet Flames, Combust. Flame, 120, 549-569 (2000)

[3] Bowman, C.T., Hanson, R.K., Davidson, D.F., Gardiner, W.C., Lissianski, V., Smith, G.P., Golden, D.M., Frenklach, M., Goldenberg, M.: GRI-Mech (2008). http://www.me.berkeley. edu/gri-mech/. Accessed February 2013

[4] Cheng, P., Dynamics of a radiating gas with application to flow over a wavy wall, AIAA Journal, 4(2), 238-245 (1966)

[5] Cuoci, A., Frassoldati A., Ferraris, G. Buzzi, Faravelli, T., Ranzi, E., The ignition, combustion and flame structure of carbon monoxide/hydrogen mixtures. Note 2: Fluid dynamics and kinetic aspects of syngas combustion, Int. J. Hydrogen Energy, 32,3486-3500 (2007)

[6] Dally, B.B., Masri, A.R., Barlow, R.S. and Fiechtner, G.J., Instantaneous and mean compositional structure of bluff- body stabilised nonpremixed flames. Combust. Flame, 114, 119–148 (1998)

[7] Dunn, M. J., Masri, A. R. and Bilger, R. W., A new piloted premixed jet burner to study strong finite-rate chemistry effects, Combust. Flame 151(1-2), 46–60 (2007)

[8] Dunn, M. J., Masri, A. R., Bilger, R. W., Barlow, R. S. and Wang, G. H., The compositional structure of highly turbulent piloted premixed flames issuing into a hot coflow, Proc. Combust. Inst. 32(2), 1779–1786 (2009)

[9] Fox, R.O., Computational models for turbulent reacting flows. Cambridge:Cambridge University Press (2003)

[10] Frassoldati, A., Faravelli, T., Ranzi, E., The ignition, combustion and flame structure of carbon monoxide/hydrogen mixtures. Note 1: Detailed kinetic modeling of syngas combustion also in presence of nitrogen compounds, Int. J. Hydrogen Energy, 32, 3471-3485 (2007)

[11] Ertesvåg, I. S. and Magnussen, B. F., The eddy dissipation turbulence energy cascade model, Combust. Sci. Technol. 159, 213–235 (2000)

[12] Hairer, E. and Wanner, G., Solving ordinary differential equations II: Stiff and differential-algebraic problems, Springer Series in Computational Mathematics, 2nd rev. ed, Springer-Verlag (1996)

[13] Hottel, H. C, and Sarofim, A.F., Radiative Transfer, McGraw-Hill, New York (1967)

[14] Geurts, B., Elements of direct and large-eddy simulation, R.T.Edwards, Philadelphia (2004)

[15] Gran, I. R. and Magnussen, B. F., A numerical study of a bluff-body stabilized diffusion flame. Part 2. Influence of combustion modeling and finite-rate chemistry, Combust. Sci. Technol. 119, 191-217. (1996)

[16] Hestens, M, Steifel, E., Methods of conjugate gradients for solving systems of algebraic equations, J. Res. Nat. Bur. Stand, 29, 409–436 (1952)

[17] Hewson, J.C., Kerstein, A.R., Stochastic simulation of transport and chemical kinetics in turbulent CO/H2/N2 flames. Combust. Theory Model., 5, 669-897 (2001)

[18] Issa, R., Solution of the implicitly discretized fluid flow equations by operator splitting, J. Comput. Phys., 62, 40–65 (1986)

[19] Jacobs, D., Preconditioned conjugate gradient methods for solving systems of algebraic equations, Tech. rep., Central Electricity Research Laboratories, Leatherhead, Surrey, England (1980)

[20] Launder B, Sharma B. Application of the energy-dissipation model of turbulence to the calculation of flow near a spinning disc. Lett. Heat Mass Transfer, 1:131–138 (1974)

[21] Launder, B. E. and Spalding, D. B., The numerical computation of turbulent flows, Comput. Method Appl. M. 3(2), 269–289 (1974)

[22] Lilleberg, B., On mathematical modeling and numerical simulation of chemical kinetics in turbulent lean premixed combustion, PhD thesis, Trondheim (2011)

[23] Kai Liu, K., Pope, S.B., Caughey, D.A., Calculations of bluff-body stabilized flames using a joint probability density function model with detailed chemistry, Combust. Flame, 141, 89–117 (2005)

[24] Lysenko, D.A., Ertesvåg, I.S. and Rian K.E., Modeling of turbulent separated flows using OpenFOAM. Comput Fluids (2012), doi:10.1016/j.compfluid.2012.01.015

[25] Magnussen, B.F., Hjertager, B.H., On mathematical modeling of turbulent combustion with special emphasis on soot formation and combustion, Proc. Combust. Inst. 16, 719–729 (1976)

[26] Magnussen, B.F., Modeling of NOx and soot formation by the Eddy Dissipation Concept. Int.Flame Research Foundation, 1st topic Oriented Technical Meeting., 17-19 Oct. 1989. Amsterdam, Holland.

[27] Marshak, R.E. Note on the spherical harmonics method as applied to the Milne problem for a sphere, Phys. Rev., 71, 443-446 (1947)

[28] Marzouk, O.A., Huckaby, E.D., A comparative study of eight finite-rate chemistry kinetics for CO/H_2 combustion, Eng. App. Comput. Fluid Mech., 4(3), 331-356 (2010)

[29] McGuirk, J.J., Rodi, W., The calculation of three-dimensional turbulent free jets. In turbulent Shear Flows I: Selected papers from the First International Symposium on Turbulent Shear Flows, editors: Durst, F., Launder, B.E., Schmidt, F.W., and Whitelaw, J.H., Springer-Verlag, Germany, 71-83 (1979)

[30] Menter, F.R., Kuntz, M., Langtry, R., Ten years of experience with the SST turbulence model. In K. Hanjalic, Y. Nagano and M. Tummers, editors, Turbulence, Heat and Mass Transfer 4, Begell House, Inc., 625-632 (2003)

[31] Vandoormaal, J.P., Raithby, G.D., Enhancements of the SIMPLE method for predicting incompressible fluid flows, Numer. Heat Transfer, 7, 147–163 (1984).

[32] Richardson, L.F., Weather prediction by numerical process. Cambridge University Press, Cambridge (1922)

[33] Sabelnikov, V., Fureby, C., LES combustion modeling for high Re flames using a multi-phase analogy, Combust. Flame, 160, 83–96 (2013)

[34] Smith, T.F., Shen, Z.F. and Friedman, J.N. , Evaluation of coefficients for the weighted sum of gray gases model, J. Heat Trans-T., ASME 104(4), 602–608 (1982)

[35] Waterson, N.P., Deconinck, H., Design principles for bounded higher-order convection schemes – a unified approach, J Comput. Phys., 224, 182–207 (2007)

[36] Weller, H.G., Tabor, G., Jasak H., Fureby, C., A tensorial approach to computational continuum mechanics using object-oriented techniques, Comp. Phys., 12(6), 620–631 (1998)

[37] Yan, J., Thiele, F., Buffat, M., A Turbulence Model Sensitivity Study for CH4/H2 Bluff-Body Stabilized Flames, Flow Turb. Combust., 73, 1–24 (2004)